Eur. Phys. J. Plus (2022) 137:526
https://doi.org/10.1140/epjp/s13360-022-02742-3

THE EUROPEAN PHYSICAL JOURNAL PLUS

Regular Article

Theoretical simulation of optical absorption coefficients in heterostructure based on semi-parabolic-double quantum wells

H. Dakhlaoui[1,2,a], **Aysevil Salman Durmuslar**[3], **I. Rodriguez-vargas**[4], **F. Ungan**[5]

[1] Nanomaterials Technology Unit, Basic and Applied Scientific Research Center (BASRC), College of Science of Dammam, Imam Abdulrahman Bin Faisal University, P. O. Box 1982, Dammam 31441, Saudi Arabia
[2] Department of Physics, College of Sciences for Girls, Imam Abdulrahman Bin Faisal University, Dammam, Saudi Arabia
[3] Department of Naval Architecture and Marine Engineering, Faculty of Engineering, Piri Reis University, 34940 Istanbul, Turkey
[4] Unidad Académica de Ciencia Y Tecnología de La Luz Y La Materia, Universidad Autónoma de Zacatecas, Carretera Zacatecas-Guadalajara Km. 6, Ejido La Escondida, 98160 Zacatecas, Zacatecas, Mexico
[5] Department of Physics, Faculty of Science, Sivas Cumhuriyet University, 58140 Sivas, Turkey

Received: 16 February 2022 / Accepted: 19 April 2022

Abstract In this work, we have performed a numerical calculation to obtain the lowest three electron subband energy levels and their density of probabilities in a n-doped heterostructure constituted by double semi parabolic quantum wells separated by square quantum well and surrounded by two outer barriers. The numerical investigation is carried out within the framework of the parabolic single band and effective mass approximations. Firstly, we have solved self-consistently the coupled Schrödinger and Poisson equations and have determined the electronic wave functions and subband energy levels. After that we have deduced the different contributions of the optical absorptions between the lowest three electron subband energy levels. The energy variations and the occupancy ratios are also discussed to show their accordance with the behavior of the total optical absorption coefficient. Throughout this study, two cases of doping were treated. The first one is a doping in the outer barriers and the second one was a doping in the inner barriers. The doping consists of inserting 1 nm of silicon layer in the middle of the barriers. The responses of different total optical absorption coefficients, subband energy levels and confining potential by increasing the concentration of the delta-doped layers are demonstrated and the two behaviors (red and blue shifted) are discussed in detail.

1 Introduction

During the last years, different research studies have proved that the geometrical shapes of quantum confining potentials as well as the added doped layers in different locations of semiconductor heterostructures present a large importance in the design and the fabrication of required optoelectronic devices operating in different emission ranges [1–11]. This importance comes from the fact that the desired emitted wavelength can be tuned by varying the concentration and location of inserted doped layers or also by changing the profile of the confining potential. The obtainment of a large diversity of heterostructures having quantum wells (QWs) with different potential shapes becomes feasible by means of the recent growth techniques such as the organic chemical vapor deposition (OCVD) and the molecular beam epitaxy (MBE) [12]. These methods make possible to create a variety of potential profiles in one, two and three dimensions.

The delta-doping technique is an efficacious method to adjust and obtain the desired values of electron and hole subband energy levels by creating additional QWs around the position of the inserted delta-doped layer. Once the doped layer is introduced, the doping atoms are ionized creating then additional triangular QWs leading to a new distribution of the subband energy levels and their corresponding wave-functions. Moreover, the delta doping strategy allows us to tune and modulate the intersubband transitions, linear and nonlinear optical properties of low-dimensional semiconductor heterostructures [13–33].

In this context, different researchers have investigated the position and concentration of delta doping layers and their effects on the electronic and optical properties of doped semiconductors. For instance, J. Osvald studied the impact of a non-central doped layer on the electronic concentration and energy levels in GaAs semiconductor and he showed that the position of the inserted doped layer affects the electronic density [34]. F. Ungan investigated the nonlinear optical properties in a single QW, and he showed that the doping concentration plays a crucial role to modify the total optical absorption coefficients (TOACs) and total refractive index changes (TRICs) [35]. The effects of double and triple $\delta-$ doped layers combined with electromagnetic fields on the optical absorption coefficients in GaAs semiconductor were studied by Dakhlaoui et al.[36]. They showed that the concentration of the doped layers can be tuned the optical absorption from the red to the blue shift. Gaggero-Sager et al. calculated the subband energy

[a] e-mail: hbaldkhlaen@iau.edu.sa (corresponding author)

Published online: 02 May 2022

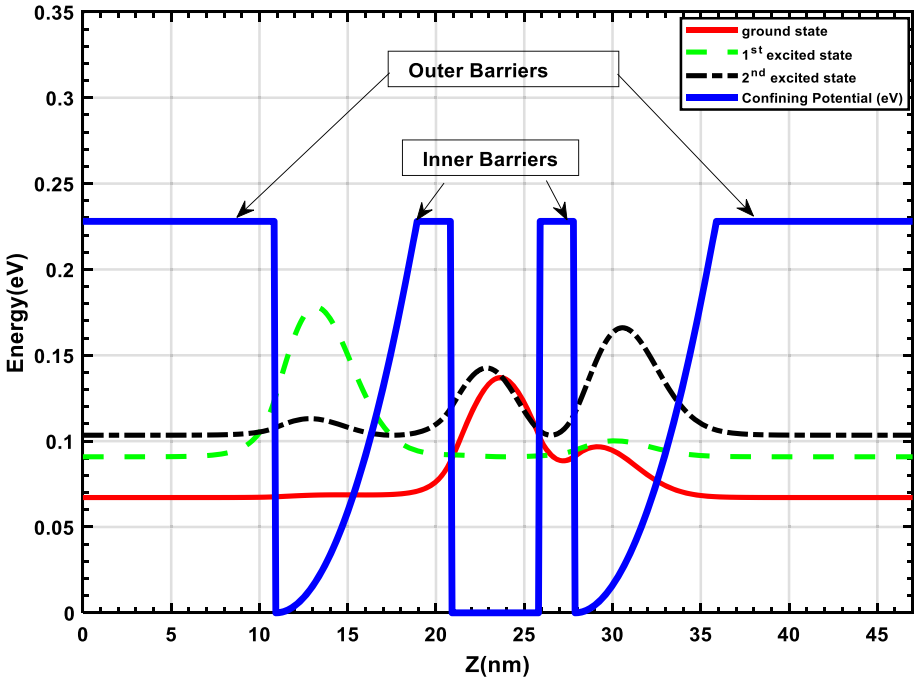

Fig. 1 Schematic diagram of the heterostructure: a square quantum well GaAs sandwiched between two semi parabolic wells and two outer AlGaAs barriers

levels in single-doped QW under the effect of temperature [37]. The influence of the hydrostatic pressure on the TOACs in n-doped GaAs was addressed by Oubram el al [38].

To the best of our knowledge, a numerical investigation of the optical absorptions produced by doped GaAs/AlGaAs double semi-parabolic QWs has not been conducted. In this paper, firstly, we will shed light on the effect of the doped layers inserted in the middle of outer barriers on the lowest three electron subband energy levels and their densities of probabilities and different optical absorption coefficients. At a second step, we will discuss the effect of the doped layers inserted in the inner barriers on the optical absorption coefficients of each transition between the lowest three levels.

Our goal is to provide to scientific community a global idea on the impact of the addition of doped layers on the optical properties in heterostructures having new shapes of confinement. The work is organized as follows: in Sect. 2, we explain our theoretical method, and we clarify the procedure or numerical resolution. In Sect. 3, we discuss and comment our theoretical findings. Finally, we give our conclusions in Sect. 4.

2 Theory

The physical problem under consideration treats the motion of electrons free to move in double semi-parabolic QWs inserted between $Al_{0.3}Ga_{0.7}As$ barriers. This structure, as shown in Fig. 1, contains two inner and outer barriers. The study addresses two cases; in the first part we consider two-doped layers in the outer barriers and in the second part we consider two-doped layers in the inner barriers. The doping consists of introducing 1 nm layer of silicon atoms in the middle of each $Al_{0.3}Ga_{0.7}As$ barrier. In accordance with the effective mass and single parabolic band approximations, the total Hamiltonian representing the electron motion can be formulated as following [36, 39, 40]:

$$H = -\frac{\hbar^2}{2m^*}\frac{d^2}{dz^2} + V_C(z) + V_H(z) \tag{1}$$

where m^* is the electron mass. $V_H(z)$ is the Hartree potential representing the electrostatic repulsion between carriers. $V_C(z)$ denotes the conduction band discontinuity between GaAs and $Al_{0.3}Ga_{0.7}As$ layers and is given by the following mathematical formulation:

$$V_C(z) = \begin{cases} V_0 & z < z_1 \\ V_0\left(\frac{z-z_1}{z_2-z_1}\right)^2 & z_1 < z < z_2 \\ V_0 & z_2 < z < z_3 \\ 0 & z_3 < z < z_4 \\ V_0 & z_4 < z < z_5 \\ V_0\left(\frac{z-z_5}{z_6-z_5}\right)^2 & z_5 < z < z_6 \\ V_0 & z_6 < z < z_7 \end{cases} \tag{2}$$

where $V_0 = 0.228$ eV. The abscissa of different interfaces separating the semiconductor layers are: $z_1 = 11$ nm; $z_2 = 19$ nm; $z_3 = 21$ nm; $z_4 = 26$ nm; $z_5 = 28$ nm; $z_6 = 36$ nm; $z_7 = 47$ nm.

The Hartree potential $V_H(z)$ in Eq. (1) denotes the supplementary conduction band resulting to the presence of two-dimensional electron gas arising from the inserted impurities in the doped layers. It is a solution of the Poisson equation given by [41–43]:

$$\frac{\mathrm{d}^2 V_H(z)}{dz^2} = \frac{e^2}{\varepsilon\varepsilon_0}\left[\frac{N_d}{\delta} - n(z)\right] \tag{3}$$

where e is the electron charge, ε_0 is the permittivity value of free space, N_d denotes the two-dimensional concentration of the silicon impurity inserted in the middle of the doped barriers. δ represents the width of the doping layer which equal to 1 nm throughout this simulation.$n(z)$ represents the density of the free electrons along the growth axis z and can be formulated as following [41, 42]:

$$n(z) = \sum_i \frac{m^* k_B T}{\pi\hbar^2} log\left[1 + \exp\left(\frac{E_F - E_i}{K_B T}\right)\right]|\Phi_i(z)|^2 \tag{4}$$

In the precedent equation, $\Phi_i(z)$ and E_i represents the wave-function and its associate energy level satisfying the equation $H\Phi_i(z) = E_i\Phi_i(z)$. k_B and T denote the Boltzmann constant and the temperature of the system, respectively. The Fermi level E_F can be deduced by solving the neutrality equation, in such a way the number of ionized ions is equal to the free electrons.

Equations (1–4) are discretized using the finite difference method and then transformed to diagonal matrices. After that, they are solved iteratively until the convergence is reached. The first step consists to determine the eigen values and eigenvectors $(E_i, \Phi_i(z))$ for arbitrary value of $V_H(z)$ by solving Eq. (1), after that these values were used to determine the electronic density $n(z)$. Finally, $n(z)$ is used again to find the new value of Hartree potential $V_H(z)_{\mathrm{new}}$. The convergence criteria was chosen such as $(V_H(z)_{\mathrm{new}} - V_H(z) < 10^{-3}$ meV). More details about the procedure of resolution can be found in our previous papers [36, 39, 40].

After finding the subband energy levels and their corresponding wave functions, we have addressed the optical absorption coefficients (linear $^{(1)}$, third-order nonlinear $^{(3)}$ and total) of the lowest three transitions $(1 \to 2)$,$(1 \to 3)$ and $(2 \to 3)$. The different contributions of the optical absorption can be written as following:

$$\alpha^{(1)}(\omega) = \omega\sqrt{\frac{\mu_0}{\varepsilon\varepsilon_0}}\frac{|M_{12}|^2\sigma_{\mathrm{if}}\hbar/\tau_{\mathrm{in}}}{(\Delta E - \hbar\omega)^2 + (\hbar/\tau_{\mathrm{in}})^2} \tag{5}$$

$$\alpha^{(3)}(\omega, I) = -2\omega\sqrt{\frac{\mu_0}{\varepsilon\varepsilon_0}}\left(\frac{I}{\varepsilon_0 n_r c}\right)\frac{|M_{12}|^4\sigma_{\mathrm{if}}\hbar/\tau_{\mathrm{in}}}{\left[(\Delta E - \hbar\omega)^2 + (\hbar/\tau_{\mathrm{in}})^2\right]^2} \times\left(1 - \frac{|M_{22} - M_{11}|^2}{4|M_{12}|^2} \times \frac{\left\{(\Delta E - \hbar\omega)^2 - (\hbar/\tau_{\mathrm{in}})^2 + 2(\Delta E)(\Delta E - \hbar\omega)\right\}}{(\Delta E)^2 + (\hbar/\tau_{\mathrm{in}})^2}\right) \tag{6}$$

The TOACs $\alpha(\omega, I)$ is given by the sum of the linear and third-order nonlinear coefficients: $\alpha(\omega, I) = \alpha^{(1)}(\omega) + \alpha^{(3)}(\omega, I)$. The term $M_{ij} = \Phi_i|ez|\Phi_j$ stands the off-diagonal dipole matrix element, μ_0 is the permeability, c is the speed of light in free space, n_r represents the refractive index, and τ_{in} is the intrasubband relaxation time. The $\Delta E = \left(E_f - E_i\right)$ term represents the energy separation between the initial and final states. σ_{if} is given by:

$$\sigma_{\mathrm{if}} = ln\left[\frac{1 + \exp(E_F - E_i/K_B T)}{1 + \exp\left(E_F - E_f/K_B T\right)}\right] \tag{7}$$

In the next section, we have considered two cases of doping. In the first part we considered a doping in the outer barriers. In the middle of each barriers we have inserted a 1 nm silicon layer with concentration equal to $N_d/2$. In the second part, we have considered the same quantities of doping concentrations but inserted in the inner barriers surrounding the square QW (Fig. 1).

3 Results and discussion

3.1 Doping in the outer barriers

In this simulation, the electron subband energy levels, confining potential, and envelope wave-functions of the system are computed by solving self-consistently the equations previously cited. The structure is constituted by a central quantum well GaAs ($L_w = 5$ nm), surrounded by two barriers $Al_{0.3}Ga_{0.7}As$ ($L_{b1} = L_{b2} = 2$ nm) followed by two semi-parabolic GaAs QWs of width ($L_{s1} = L_{s2} = 8$ nm). The outer barriers, as showed in Fig. 1, has a constant width equal to 11 nm. The parameters used throughout this simulation are:$T = 300K; n_r = 3.2; T_{12} = 0.14ps; \Gamma_{12} = 1/T_{12}; \mu = 4\pi \times 10^{-7}$ H.m^{-1}; $m^* = 0.067$ m$_0$. We assume the same electron mass in all wells and barriers regions. The confining potential which describes the continuity between $Al_xGa_{(1-x)}As$ and GaAs semiconductors is given by the following expression [43]:$V_{\mathrm{conf}}(x) = 600 \times \left(1.155x + 0.37x^2\right)$. In the following section, we considered two doping silicon layers placed in the middle of the outer barriers, with each layer having a width of 1 nm. Our

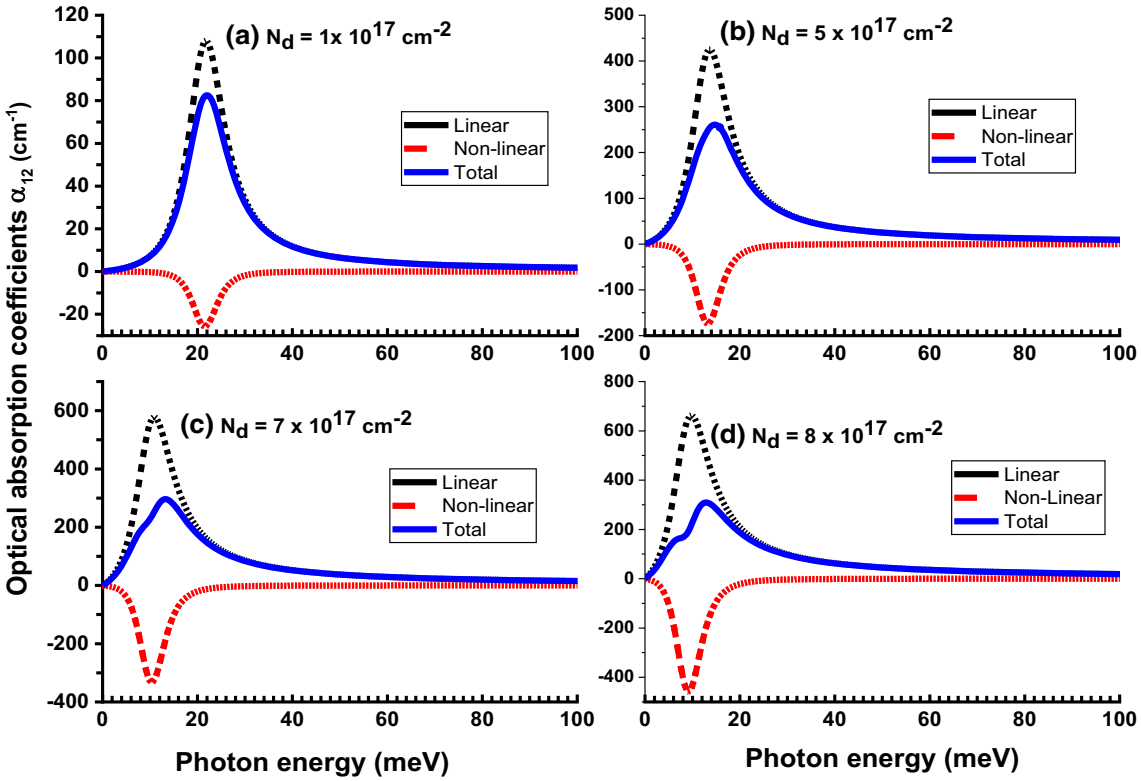

Fig. 2 Linear, nonlinear and total optical absorption coefficients (α_{12}) for different doping concentrations in the outer barriers

aim is to study the impact of these impurities on the linear and nonlinear optical absorption coefficients which is illuminated by an incident optical intensity $I = 0.3$ MW/cm^2.

In Fig. 2a–d, we display the linear, third-order nonlinear and TOACs of the transition between the ground and the first excited states ($1 \rightarrow 2$) depending on the incident photon energy for four different concentrations $N_d = 1, 5, 7$ and 8×10^{17} cm^{-2}. It is clear from all these figures that the nonlinear contributions present an opposite variation compared to the linear ones. As consequence the TOACs are reduced in all cases. In other words, the nonlinear contributions must be taken into consideration. In addition, we observe that when N_d rises, the amplitudes of both linear and nonlinear contributions increase, but the nonlinear coefficients increase larger than those of the linear coefficients which leads to the apparition of a bleaching for N_d equal to 7 and 8×10^{17} cm^{-2}. Furthermore, we observe a redshift of all coefficients by increasing N_d. In fact, the abscissa corresponding to the peaks of different coefficients was located around 21 meV for N_d equal to 1×10^{17} cm^{-2} and then they move progressively to lower values until they touch 8 meV for N_d equal to 8×10^{17} cm^{-2}. In Fig. 3a–d, we display the linear, third-order nonlinear and TOACs of the transition between the ground and the second excited states ($1 \rightarrow 3$) depending on the incident photon energy for four different concentrations $N_d = 1, 5, 7$ and 8×10^{17} cm^{-2}. Again, by examining these figures, we conclude that all contributions of absorption coefficients relative to the transition ($1 \rightarrow 3$) present a redshift with the incident energy by increasing the values of N_d. The nonlinear contributions in this transition are less than those observed in ($1 \rightarrow 2$) transition, as a result, the bleaching effect is not occurred in these figures. We remark that the total coefficient in each case presents an increase with the values of N_d. The optical absorption coefficients related to ($2 \rightarrow 3$) transitions are given by Fig. 4a–d. Contrarily to the previous transitions ($1 \rightarrow 2$) and ($1 \rightarrow 3$), this transition presents a blue shift. In fact, by increasing the incident photon energy, we observe that all coefficients (linear, nonlinear and total) move toward higher energies. Again, we observe that the nonlinear contribution is important and it must be taken into consideration.

The red and blue shifts behavior and the variation of the peaks of each coefficient (linear, nonlinear and total) can be justified and interpreted by studying the variation of the energy variation $\Delta E_{ij} = (E_j - E_i)$ and the occupancy function f_{ij}.

In Fig. 5, we display the variation of the energy separations between the lowest three levels as a function of the doping concentrations N_d. It is clear that the two energy separations $(E_2 - E_1)$ and $(E_3 - E_1)$ diminish progressively with N_d which confirms the red shift observed in the previous figures of all coefficients of these transitions. In addition, the decrease of $(E_2 - E_1)$ is faster than of $(E_3 - E_1)$. In this figure we observe clearly that $(E_3 - E_2)$ rises by increasing N_d which confirms the blue shift already observed in Fig. 4a–d.

The maxima variation of the total apical absorption coefficient for each transition is governed by the occupancy function f_{ij} which is plotted in Fig. 6. It is clear that f_{12}, f_{13} and f_{23} present an ascending behavior as a function of N_d. This increase in f_{ij}

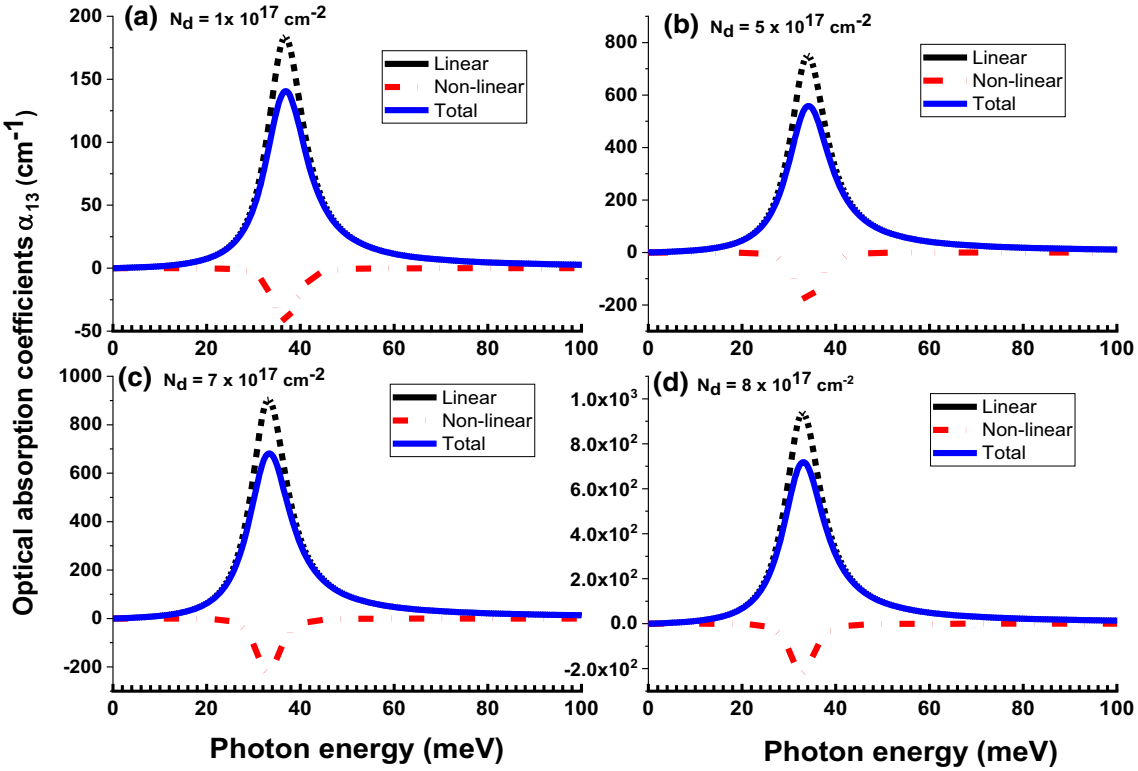

Fig. 3 Linear, nonlinear and total optical absorption coefficients α_{13} for different doping concentrations in outer barriers

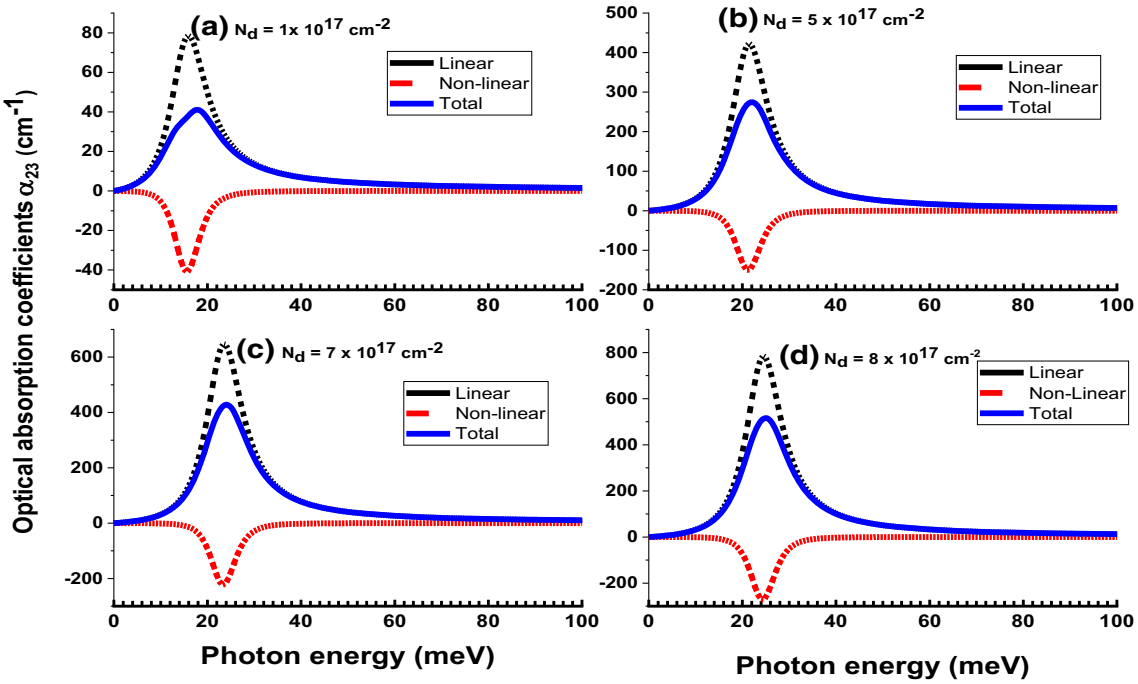

Fig. 4 Linear, nonlinear and total optical absorption coefficients α_{23} for different doping concentrations in the outer barriers

explains the rising of the total optical absorption coefficient observed in all transitions in the previous figures. f_{12} is higher than f_{23} at $N_d = 1 \times 10^{17}\,\mathrm{cm}^{-2}$, but for $N_d = 8 \times 10^{17}\,\mathrm{cm}^{-2}$, f_{23} becomes dominant. This explains in turn the values of the (TOAC) maximums observed in Figs. 2 and 4. In fact, for $N_d = 1 \times 10^{17}\,\mathrm{cm}^{-2}$, $\alpha_{12(\max)} = 83\,\mathrm{cm}^{-1}$ and $\alpha_{23(\max)} = 41\,\mathrm{cm}^{-1}$, however, for $N_d = 8 \times 10^{17}\,\mathrm{cm}^{-2}$, these values becomes $\alpha_{12(\max)} = 309\,\mathrm{cm}^{-1}$ and $\alpha_{23(\max)} = 512\,\mathrm{cm}^{-1}$. Per consequent the value of the doping concentration has a great importance to determine the maxima of the TOACs. In addition, we can observe that f_{13} is larger

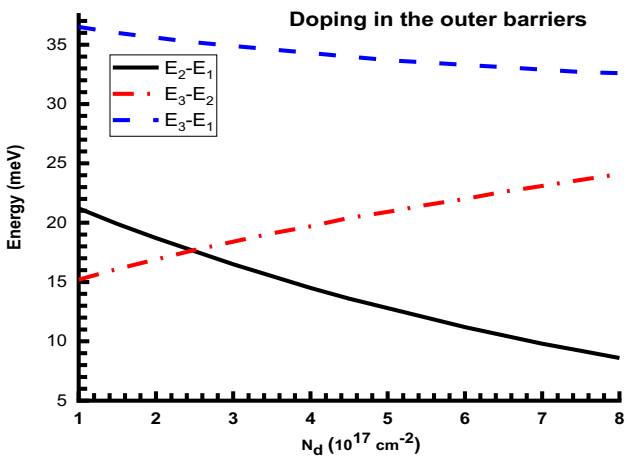

Fig. 5 Variations of the energy separations as a function of the doping concentration N_d injected into outer barriers

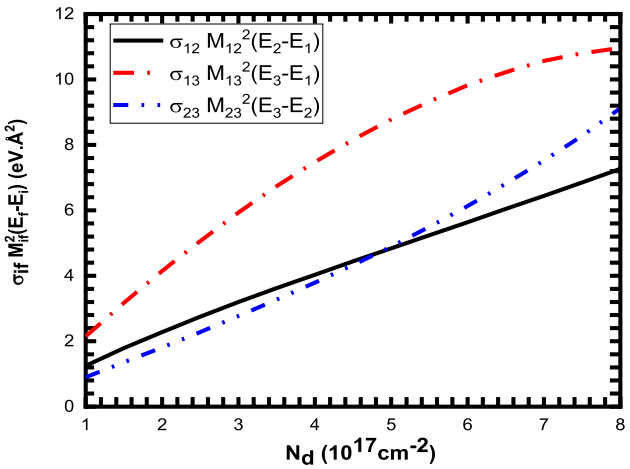

Fig. 6 variation of the occupancy function *fij* for doped outer barriers

than f_{12} and f_{23} for all values of N_d. This traduces the large amplitudes of the total optical absorption $\alpha_{13(\max)}$ which increases rapidly with N_d until it reaches the value 730 cm^{-1} for $N_d = 8 \times 10^{17}\ \mathrm{cm}^{-2}$. Furthermore, we observe that f_{13} presents a tendency toward constant value between $7 \times 10^{17}\ \mathrm{cm}^{-3}$ and $8 \times 10^{17}\ \mathrm{cm}^{-2}$. This behavior is attributed essentially to the matrix element M_{13}^2 which presents a constant value for $N_d > 7 \times 10^{17}\ \mathrm{cm}^{-2}$. In fact, for higher doping concentrations the two wave-functions Ψ_1 and Ψ_3 arrive to a saturate overlap between them, as a result, the matrix element M_{13}^2 goes to a constant value.

In Fig. 7a, b, we display the electronic density and the energy levels together with the confining potential for two values of the doping concentrations $N_d = 1 \times 10^{17}\ \mathrm{cm}^{-2}$ and $4 \times 10^{17}\ \mathrm{cm}^{-2}$. The amount of N_d is divided on two layers of width 1 nm. Each layer is inserted in the middle of the outer barriers. By examining Fig. 7a, b, it is clear that the confining potential in the outer barriers which was flat in the absence of doping, tilts and present a small triangular well around the inserted doped layer at the middle of each barrier. It is clear also that the ionized silicon atoms supply free electrons which are transmitted along the structure. As shown in these figures, the electronic density is important at the central well and presents two spread in the two semi-parabolic wells. But the density in the left well is more intense than the right one.

3.2 Doping in the inner barriers

In this section, we consider the same amount of the doping concentration used in the previous section but here we introduced doped layers in the inner barriers. We divide N_d in two equal values. Each one is inserted at the middle of the inner barriers. Figure 8a–d shows the linear, nonlinear and total optical absorption coefficients of the $(1 \rightarrow 2)$ transition as a function of the incident photon energy. It is clear that all the coefficients twist toward higher energies suffering a blue shift behavior. The amplitudes of nonlinear coefficients are less than those of the linear contributions and the bleaching is absent. However, this transition has showed a bleaching in the total optical absorption in the previous section when we considered the doping in the outer barriers. this bleaching was clear for $N_d = 7 \times 10^{17}\ \mathrm{cm}^{-2}$ and $8 \times 10^{17}\ \mathrm{cm}^{-2}$. As a result, the amplitudes of the nonlinear optical absorption coefficients are reduced by doping in the inner barriers compared to the outer barriers. Furthermore, we observe that maximum of the total optical absorption increases strongly with increasingN_d. For $N_d = 1 \times 10^{17}\ \mathrm{cm}^{-2}$ the absorption is $\alpha_{12(\max)} = 200\ \mathrm{cm}^{-1}$, but it can reach 2400 cm^{-1} for $N_d = 8 \times 10^{17}\ \mathrm{cm}^{-2}$.

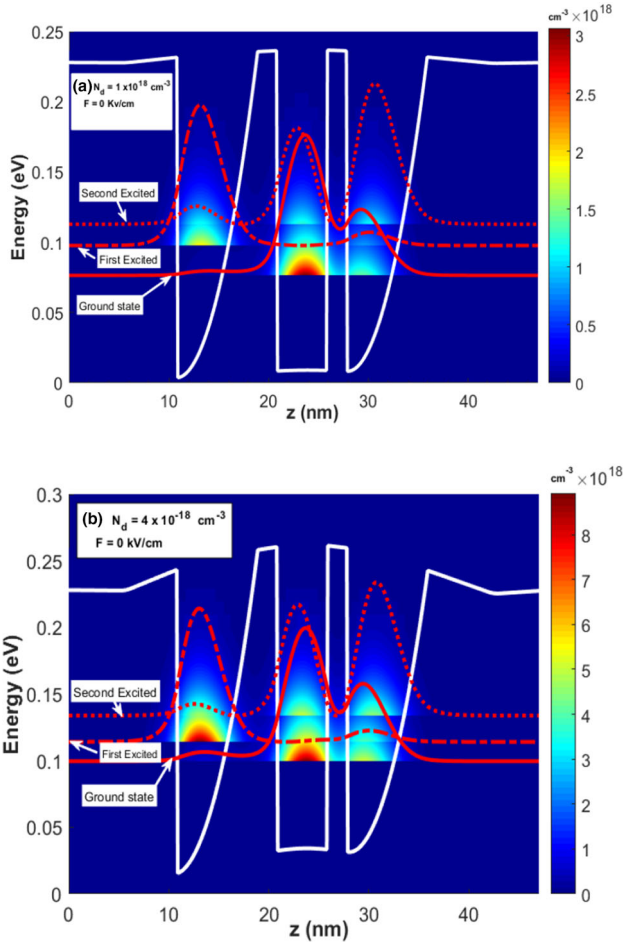

Fig. 7 Electronic density and density of probabilities for two doping concentration **a** 1×10^{17} cm^{-2}, **b** 4×10^{17} cm^{-2}

We plot in Fig. 9a–d, the linear, nonlinear and total optical absorption coefficients of the $(1 \rightarrow 3)$ transition as a function of the incident photon energy. Similarly, as $(1 \rightarrow 3)$ transition, all the coefficients of $(1 \rightarrow 3)$ transition display a blue shift behavior since they moved toward low energies for doped outer barriers. The nonlinear coefficient presents comparatively small amplitudes for all values of N_d. For instance, at $N_d = 8 \times 10^{17} cm^{-2}$, the nonlinear coefficient is negligible compared to the linear one. As a result, the total optical absorption coefficient is close to the linear one. Therefore, the higher doping concentration in the inner barriers permits only the linear absorption coefficients and switch-off the nonlinear coefficients.

The linear, nonlinear and total optical absorption coefficients of the $(2 \rightarrow 3)$ transition as a function of the incident photon energy is reported in Fig. 10a–c. It is clear that contrarily to α_{12} and α_{13} which present a blue shift, here all the coefficients of α_{23} present a red shift behavior. In fact, all of them move toward lower energies by increasing N_d. The nonlinear absorption coefficient increases with N_d and strongly affects the total optical absorption coefficient. The bleaching effect is clearly seen for all values of N_d. All these variations observed in the abscissa and amplitude of each absorption coefficient can be justified and interpreted by studying the energy separations and the occupancy ratios between the energy levels.

To do this, we have addressed the variation of the energy separations $(E_2 - E_1)$, $(E_3 - E_1)$ and $(E_3 - E_2)$ as a function of the photon incident energy as presented by Fig. 11. $(E_2 - E_1)$ and $(E_3 - E_1)$ increase almost linearly with N_d justifying the blue shift behavior previously detected in all variations of the coefficients of α_{12} and α_{13} as seen in Figs. 8 and 9. However, the $(E_3 - E_2)$ decreases slowly with N_d especially for $4 \times 10^{18}\, cm^{-3} < N_d < 8 \times 10^{18}\, cm^{-3}$. This reduction in $(E_3 - E_2)$ with N_d is in accordance with the red shift exhibited by α_{23} as shown by Fig. 10.

The evolution of the amplitudes of each absorption coefficient can be interpreted by the occupancy ration f_{ij}. In Fig. 12, we plot f_{12}, f_{13} and f_{23} as a function of the doping concentration N_d. As shown in this Fig. 12, f_{12} rises promptly with N_d. This behavior confirms the rapid increase of the peak $(\alpha_{12})_{max}$ observed in Fig. 8. We remark also that f_{23} rises with N_d but its increase is lower than of f_{12}. This weak increment is obviously illustrated in the variation of $(\alpha_{23})_{max}$ which tends to constant value for $N_d > 4 \times 10^{18}\, cm^{-3}$. Contrarily to f_{12} and f_{23}, the occupancy ratio f_{13} increases at first until a certain constant obtained for $N_d = 3.5 \times 10^{18}\, cm^{-3}$. After that it diminishes progressively. This diminution explains clearly the behavior of the peak of the total absorption coefficient $(\alpha_{13})_{max}$. In fact, $(\alpha_{13})_{max}$ starts from 275 cm^{-1} for $N_d = 1 \times 10^{18}\, cm^{-3}$, rises until it reaches 650 cm^{-1}

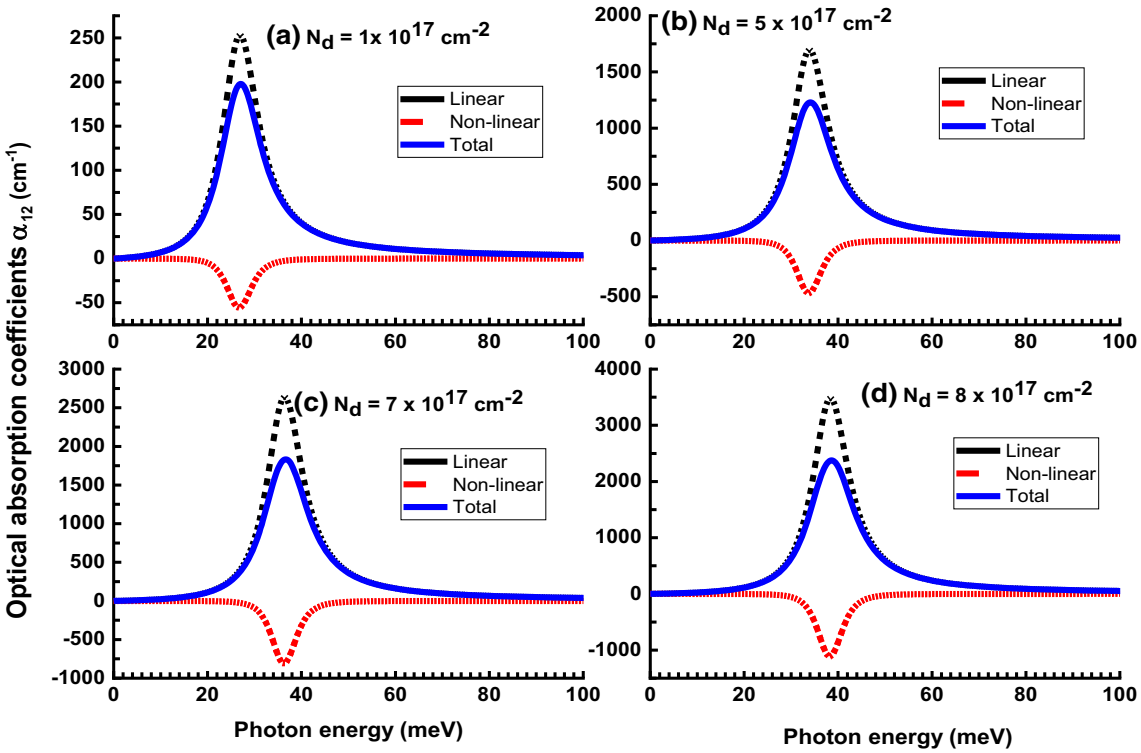

Fig. 8 Linear, nonlinear and total optical absorption coefficients α_{12} for different doping concentrations in inner barriers

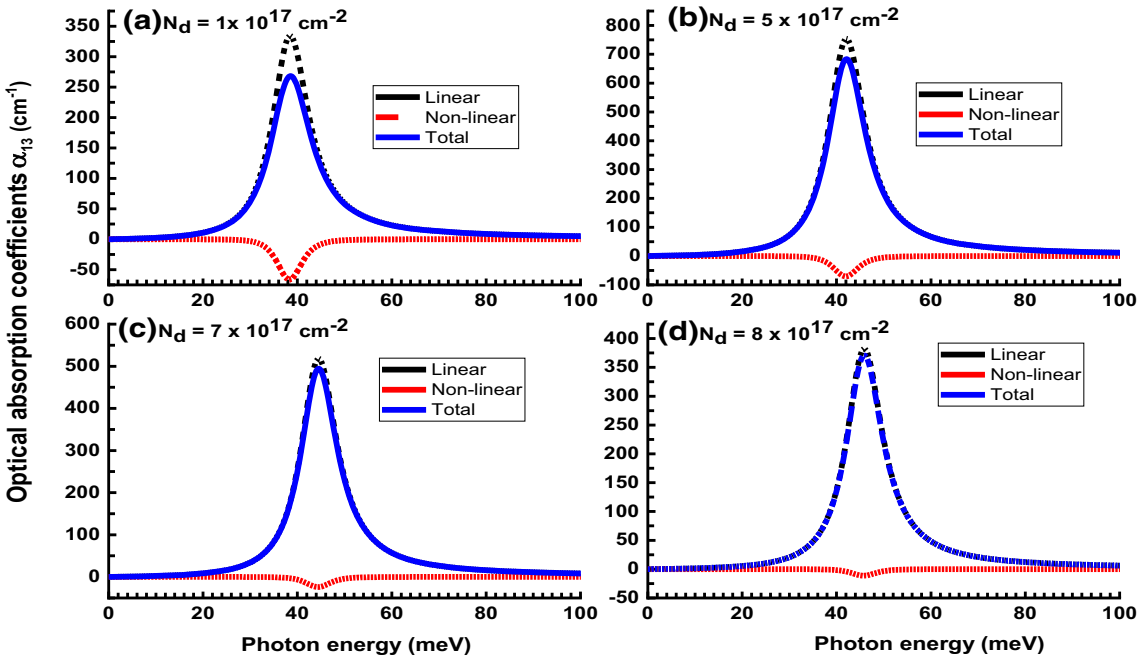

Fig. 9 Linear, nonlinear and total optical absorption coefficients α_{13} for different doping concentrations in inner barriers

for $N_d = 5 \times 10^{18}$ cm^{-3} and finally, it is reduced to 375 cm^{-1} for$N_d = 8 \times 10^{18}$ cm^{-3}. This behavior observed in (α_{13}) absorption is very interesting since it permits us to adjust the maximum of absorption by selecting appropriately the doping concentration.

By examining all the previous results, we observe that the location of the doped layers presents an ultimate procedure to obtain the desired energy variations($E_f - E_i$), and thus the desired shift (red or blue shift) when we increment the concentrationN_d. For instance, as observed in Fig. 5, when the impurities are inserted in the outer barriers, increase of the concentration N_d produces a decrease of $(E_2 - E_1)$ and $(E_3 - E_1)$, while $(E_3 - E_2)$ increases considerably. However, when the impurities are located in

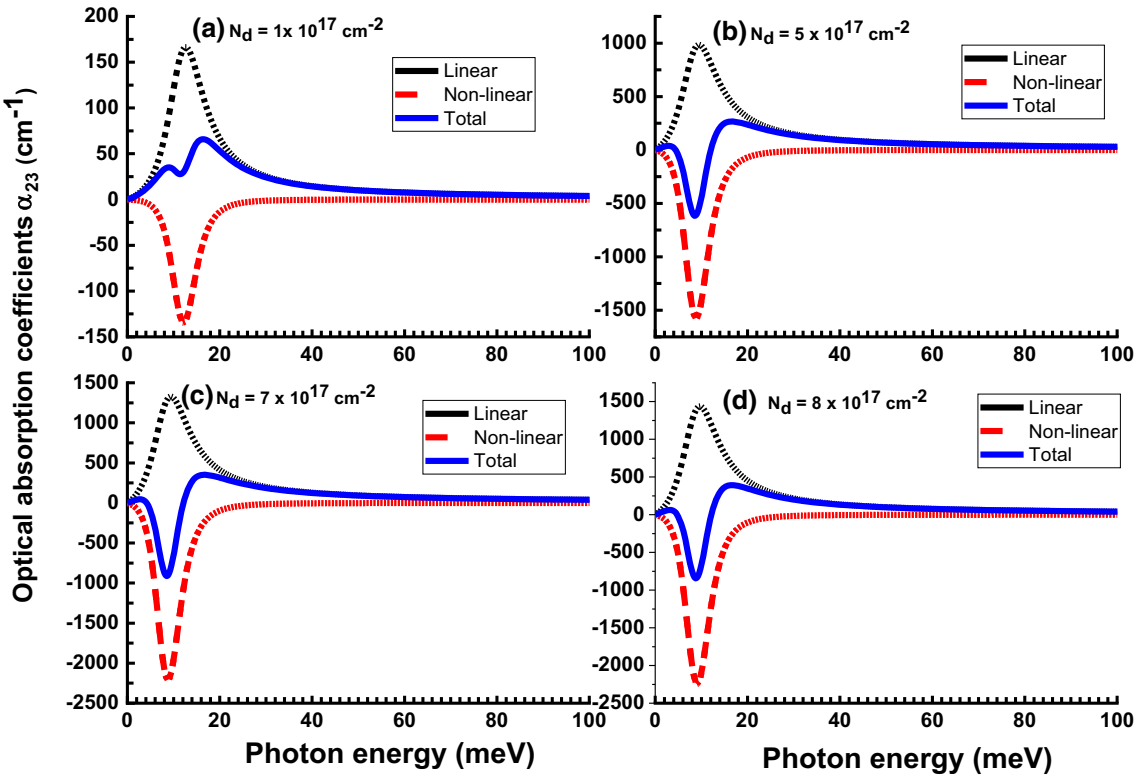

Fig. 10 Linear, nonlinear and total optical absorption coefficients α_{23} for different doping concentrations in inner barriers

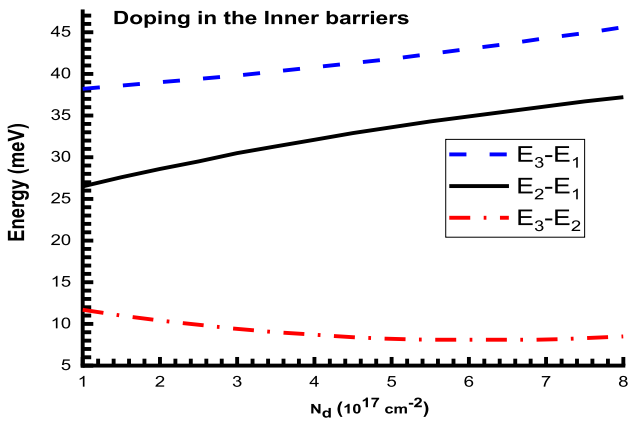

Fig. 11 Variations of the energy separations as a function of the doping concentration N_d injected into inner barriers

the inner barriers, an increase ofN_d, produces an inverse variation. In fact, as shown in Fig. 11, when N_d rises, $(E_2 - E_1)$ and $(E_3 - E_1)$ increase their values, while $(E_3 - E_2)$ diminishes gradually. These behaviors of variations in each case of doping are responsible to the blue or red shifts observed in each optical absorption coefficients. Hence, moving the doping layers from the inner to outer barriers can be a suitable strategy used by the experimentalist to obtain the desired variation in different optical absorption coefficients.

The study of the optical properties in symmetric double semi-parabolic quantum wells was also investigated by Keshavarz et al. [44]. Their findings demonstrated that the optical absorption coefficients can be red and blue shifted by adjusting the quantum size of the heterostructure such as the width of the quantum wells and barriers. Their work was limited to the transition between the ground and the first excited states $(E_1 \rightarrow E_2)$. We believe that the present work which treats the optical absorptions between three levels (E_1, E_2 and E_3) can provides additional solution to the experimentalist and this by manipulating the location and concentrations of the inserted doped layers.

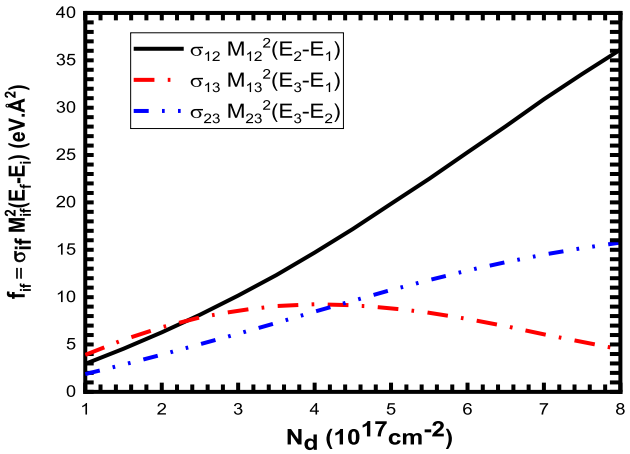

Fig. 12 Variation of the occupancy function f_{ij} for doped inner barriers

4 Conclusion

Within the effective mass and parabolic approximations, we have calculated the different optical absorption coefficients between the lowest three energy levels in a doped heterostructure based on semi parabolic quantum wells. The resolution of the differential equations describing the physics of the problem was based on the finite difference method. Firstly, we have calculated the energy levels, the confining potential and the density of probabilities. Two doping cases were investigated; a doping in the inner barriers and a doping in the outer barriers. The energy separations and the occupancy functions controlling the variation of the (TOAC) were discussed in detail. The obtained results show that in the case of the doping in outer barrier, an increase of the donor's concentration favorize a red shift of $(1 \rightarrow 2)$ and $(1 \rightarrow 3)$ transitions. However, the $(2 \rightarrow 3)$ transition exhibits a blue shift behavior. Furthermore, we have shown that the doping in the inner barriers produces a contrarily shifts compared to that obtained with doping in the outer barriers. In fact, $(1 \rightarrow 2)$ and $(1 \rightarrow 3)$ transitions exhibit a blue shift. But $(2 \rightarrow 3)$ transition displayed a red shift.

These findings permit us to tune the present system only by modifying the locations and densities of the inserted doped layers without need to any applied external fields. The desired positions and the amplitudes of the (TOAC) can be obtained by only increasing the concentrations of each doped layers. We expect that the obtained results in this research motivate future experimental studies related with doping techniques in semiconductor materials.

Data availability This work is new and all the results are computed from the equations. The data that support the findings of this study are available from the corresponding author upon reasonable request.

References

1. J. Krupski, M. PiPetka, Solid State Commun. **107**, 141 (1998)
2. E. Ozturk, Y. Ergun, H. Sari, I. Sokomen, Appl. Phys. A **73**, 749 (2001)
3. E. Kasapoglu, F. Ungan, H. Sari, I. Sökmen, Phys. E **42**, 1623 (2010)
4. N. Raigoza, A.L. Morales, C.A. Duque, Braz. J. Phys. **36**, 350 (2006)
5. M.G. Barseghyan, A.A. Kirakosyan, C.A. Duque, Phys. Status Solidi (b) **246**, 626 (2009)
6. J.C. Martínez-Orozco, I. Rodríguez-Vargas, C.A. Duque, M.E. Mora-Ramos, L.M. Gaggero-Sager, Phys. Status Solidi (b) **246**, 581 (2009)
7. J.C. Martínez-Orozco, I. Rodríguez-Vargas, M.E. Mora-Ramos, C.A. Duque, Microelectron. J. **39**, 648 (2008)
8. O. Oubram, M.E. Mora-Ramos, L.M. Gaggero-Sager, Eur. Phys. J. B **71**, 233 (2009)
9. I. Rodríguez-Vargas, M.E. Mora-Ramos, C.A. Duque, Microelectron. J. **39**, 438 (2008)
10. P. Nithiananthi, K. Jayakumar, Phys. Status Solidi (b) **246**, 1238 (2009)
11. R. Khordad, S. Kheiryzadeh Khaneghah, M. Masoumi, Superlattices Microstruct. **47**, 538 (2010)
12. M.K. Gurnick, T.A. De Temple, IEEE J. Quantun Electron. QE- **19**, 791 (1983)
13. Z. Zhang, K. Guo, S. Mou, B. Xiao, Y. Zhou, Nonlinear optical properties in square tangent quantum wells. Optik **127**, 928–933 (2016)
14. S. Ridene, Infrared Phys. Technol. **89**, 218 (2018)
15. L.M. Gaggero-Sager, R. Perez-Alvarez, J. Appl. Phys. **78**, 4566 (1995)
16. I. Rodriguez-Vargas, L.M. Gaggero-Sager, V.R. Velasco, Surf. Sci. **537**, 75 (2003)
17. S. Almansour, H. Dakhlaoui, E. Algrafy. Chin. Phys. Lett., 33 (2016), Article 027301
18. H. Ben Bechir Dakhlaoui, N. Mouna, Chem. Phys. Lett. **693**, 40 (2018)
19. Z.D. Chakhnakia, L.V. Khvedelidze, N.P. Khuchua, R.G. Melkadze, G. Peradze, T.B. Sakharova, Z. Hatzopoulos, Proc. SPIE **5401**, 354 (2004)
20. R.S. Balmer, J.R. Brandon, S.L. Clewes, H.K. Dhillon, J.M. Dodson, I. Friel, P.N. Inglis, T.D. Madgwick, M.L. Markham, T.P. Mollart, N. Perkins, G.A. Scarsbrook, D.J. Twitchen, A.J. Whitehead, J.J. Wilman, S.M. Woollard, J. Phys. Condens. Matter **21**, 364221 (2009)
21. O. Oubram, L.M. Gaggero-Sager, Prog. Electromagn. Res. L **2**, 81 (2008)
22. Y.M. Lin, S.L. Wu, S.J. Chang, S. Koh, Y. Shiraki, IEEE Electron. Device Lett. **24**, 69 (2003)
23. H. Dakhlaoui, Optik **124**, 3726 (2013)
24. R. Said, Superlattice Microstruct. **114**, 379 (2018)

25. M.H. Degani, Phys. Rev. B **44**, 5580 (1991)
26. H. Dakhlaoui, Optik **168**, 416 (2018)
27. H. Saidi, R. Said, Superlattice Microstruct. **98**, 504 (2016)
28. E. Ozturk, H. Sari, Y. Ergun, I. Sokmen, Eur. Phys. J. Appl. Phys. **21**, 91 (2003)
29. E. Ozturk, Y. Ergun, H. Sari, I. Sokmen, Superlattice Microstruct. **28**, 35 (2000)
30. E. Ozturk, Y. Ergun, H. Sari, I. Sokmen, J. Appl. Phys. **91**, 2118 (2002)
31. X. Zheng, T.K. Carns, K.L. Wang, B. Wu, Appl. Phys. Lett. **62**, 504 (1993)
32. K. Mao-Long, J.S. Rimmer, B. Hamilton, J.H. Evans, M. Missous, K.E. Singer, P. Zalm, Phys. Rev. B **45**, 14114 (1992)
33. R. Said, Chem. Phys. Lett. **702**, 44–48 (2018)
34. J. Osvald, Phys. E. **23**, 147 (2004)
35. F. Ungan, J. Lumin. **131**, 2237 (2011)
36. H. Dakhlaoui, M. Nefzi, Superlattice Microstruct. **136**, 106292 (2019)
37. L.M. Gaggero-Sager, G.G. Naumis, M.A. Munoz-Hernandez, V. Montiel-Palma, Phys. B **405**, 4267 (2010)
38. O. Oubram, O. Navarro, L.M. Gaggero-Sager, J.C. Martínez-Orozco, I. Rodríguez-Vargas, Solid State Sci. **14**, 440 (2012)
39. H. Dakhlaoui, I. Altuntas, M.E. Mora-Ramos, F. Ungan, Eur. Phys. J. Plus **136**, 1–15 (2021)
40. H. Dakhlaoui, Chin. Phys. B **23**, 097304 (2014)
41. H. Dakhlaoui, Opt. Photonics J. **2**, 22491 (2012)
42. A. Shaffa, D. Hassen, A. Emane, Chin. Phys. B **33**, 027301 (2016)
43. H. Dakhlaoui, M. Nefzi, Res. Phys. **15**, 102618 (2019)
44. A. Keshavarz, M.J. Karimi, Phys. Lett. A **374**, 2675 (2010)